

## Journal Pre-proofs

### Hit-to-Lead Optimization and Discovery of a Potent, and Orally Bioavailable G Protein Coupled Receptor Kinase 2 (GRK2) Inhibitor

Guozhang Xu, Michael D. Gaul, Zhijie Liu, Renee L. DesJarlais, Jenson Qi, Weixue Wang, Daniel Krosky, Ioanna Petrounia, Cynthia M. Milligan, An Hermans, Hua-Rong Lu, Devine Zheng Huang, June Zhi Xu, John C. Spurlino

PII: S0960-894X(20)30713-7  
DOI: <https://doi.org/10.1016/j.bmcl.2020.127602>  
Reference: BMCL 127602

To appear in: *Bioorganic & Medicinal Chemistry Letters*

Received Date: 8 August 2020  
Revised Date: 26 September 2020  
Accepted Date: 1 October 2020

Please cite this article as: Xu, G., Gaul, M.D., Liu, Z., DesJarlais, R.L., Qi, J., Wang, W., Krosky, D., Petrounia, I., Milligan, C.M., Hermans, A., Lu, H-R., Huang, D.Z., Xu, J.Z., Spurlino, J.C., Hit-to-Lead Optimization and Discovery of a Potent, and Orally Bioavailable G Protein Coupled Receptor Kinase 2 (GRK2) Inhibitor, *Bioorganic & Medicinal Chemistry Letters* (2020), doi: <https://doi.org/10.1016/j.bmcl.2020.127602>

This is a PDF file of an article that has undergone enhancements after acceptance, such as the addition of a cover page and metadata, and formatting for readability, but it is not yet the definitive version of record. This version will undergo additional copyediting, typesetting and review before it is published in its final form, but we are providing this version to give early visibility of the article. Please note that, during the production process, errors may be discovered which could affect the content, and all legal disclaimers that apply to the journal pertain.

© 2020 Published by Elsevier Ltd.



**Hit-to-Lead Optimization and Discovery of a Potent, and Orally Bioavailable G Protein  
Coupled Receptor Kinase 2 (GRK2) Inhibitor**

Guozhang Xu<sup>a\*</sup>, Michael D. Gaul<sup>a</sup>, Zhijie Liu<sup>a</sup>, Renee L. DesJarlais<sup>a</sup>, Jenson Qi<sup>b</sup>, Weixue Wang<sup>a</sup>, Daniel Krosky<sup>a</sup>, Ioanna Petrounia<sup>a</sup>, Cynthia M. Milligan<sup>a</sup>, An Hermans<sup>c</sup>, Hua-Rong Lu<sup>c</sup>,  
Devine Zheng Huang<sup>b</sup>, June Zhi Xu<sup>b</sup>, and John C. Spurlino<sup>a</sup>

<sup>a</sup>Discovery Sciences, <sup>b</sup>Cardiovascular & Metabolic Research, Janssen Research & Development, L.L.C., Welsh & McKean Roads, Spring House, PA 19477, and <sup>c</sup>Discovery Sciences, Janssen Research & Development, LLC, Turnhoutseweg 30, 2340 Beerse, Belgium

Corresponding Author

Guozhang Xu, Ph.D.

Tel.: +1 215 628 7940

E-mail address: [gxu4@its.jnj.com](mailto:gxu4@its.jnj.com) (G. Xu)

Janssen Research & Development

Discovery Sciences

SH 42-2314

1400 McKean Road

Spring House, PA 19477

Congestive heart failure (HF) due to cardiac injury or insult is a complex disease associated with ventricular remodeling, excessive neurohormonal stimulation, abnormal Ca<sup>2+</sup> handling, and proliferation of the extracellular matrix.<sup>1,2</sup> One key characteristic of HF is that the heart cannot

effectively pump enough blood to meet the body's needs due to its inability to produce a strong myocardial contraction (pumping capacity). In the United States, there are 6.5 million adults diagnosed with HF.<sup>3</sup> Current treatments including angiotensin converting enzyme (ACE) inhibitors, angiotensin II receptor antagonists,  $\beta$ -adrenergic receptor ( $\beta$ -AR) blockers, diuretics, and calcium channel blockers can only lead to modest improvement in survival rates.<sup>4,5</sup> There remains an unmet need for novel and effective HF therapies.

It is well known that the sympathetic nervous system increases the levels of circulating catecholamines (CA) such as norepinephrine and epinephrine as one of the neurohormonal compensatory mechanisms in response to the failing heart.<sup>6</sup> These endogenous hormones bind to  $\beta$ -adrenergic receptors ( $\beta$ ARs) on the surface of cardiomyocytes, leading to an increase in intracellular cyclic adenosine 3',5'-monophosphate (cAMP) levels, which in turn mediates the positive inotropic effect manifested as enhanced myocardial contraction.<sup>7</sup> In the short term, this will compensate for compromised myocardial contractile function and maintain the cardiovascular homeostasis. However, continuous release of catecholamines and persistent  $\beta$ -AR activation will lead to progressive cardiac remodeling and worsening function.<sup>8</sup> G-protein receptor kinase 2 (GRK2), an intracellular serine/threonine protein kinase and the major isoform of GRK in cardiac myocytes, mediates the phosphorylation of the serine and threonine residues on the cytoplasmic loops or tails of  $\beta$ -ARs, promotes the binding of  $\beta$ -arrestin to the phosphorylated receptor, which sterically hinders the coupling between the G-proteins and the receptor and leading to functional desensitization, as well as subsequently facilitates the internalization of the receptor.<sup>9</sup> GRK2 expression is up-regulated in the failing human heart and leads to downregulation and desensitization of the  $\beta$ -ARs, which further increases CA secretion and drives HF progression in a deleterious feedback fashion.<sup>10</sup>

One would anticipate that inhibition of GRK2 will disrupt the internalization of  $\beta$ -ARs, leading to an increase in activated  $\beta$ -ARs, and allow the heart to remain responsive to the sympathetic nervous system. It has been shown that GRK2 inhibition by either overexpression of the  $\beta$ ARKct, the peptide inhibitor of GRK2, or cardiac specific GRK2 gene ablation, improved cardiac function and survival with increases in  $\beta$ -AR density and  $\beta$ -AR responses in several HF

models.<sup>11-13</sup> Targeting GRK2 with orally bioavailable small molecule inhibitors represents a potentially attractive mechanism for the treatment of HF.<sup>14,15</sup>

In the past decade, significant medicinal chemistry efforts have been made to develop GRK2 inhibitors and representative compounds are shown in Figure 1. Balanol<sup>16</sup> and Takeda **103A**<sup>17</sup> compete with ATP for binding to the GRK2 active site, although Takeda **103A** exhibits greater inhibitory activity on GRK2. Interestingly, paroxetine, a selective serotonin inhibitor, was identified to have modest GRK2 inhibitory activity.<sup>18</sup>

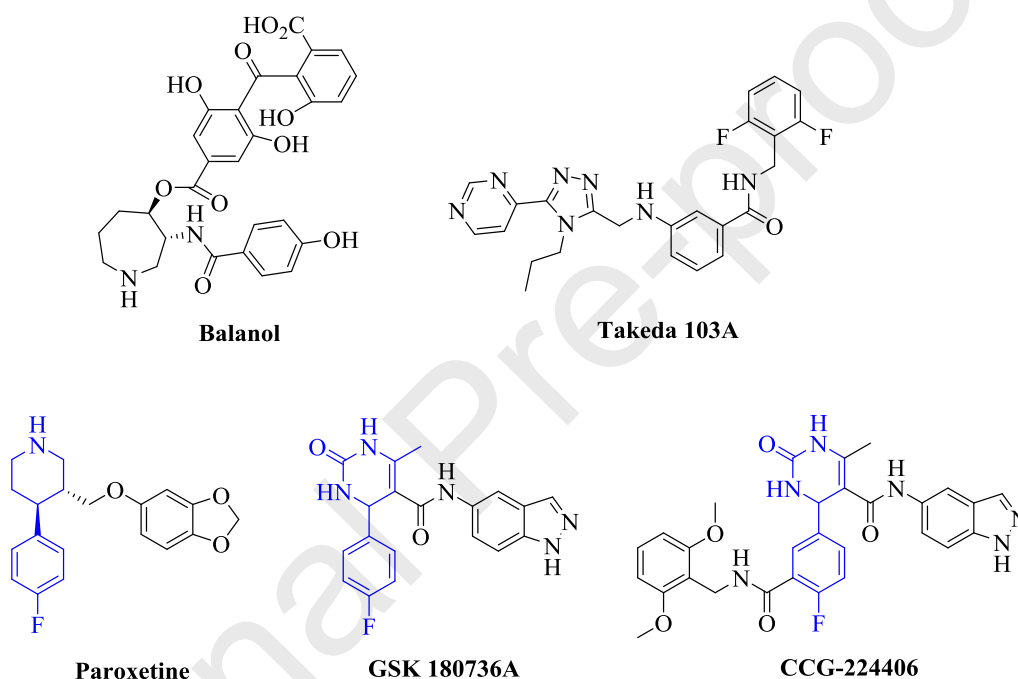


**Figure 1.** Representative GRK2 inhibitors in the literature

Several paroxetine-related derivatives including **GSK180736A** and **CCG-224406** were reported with improved GRK2 inhibitory activity.<sup>19, 20</sup> However, neither **GSK180736A** nor **CCG-224406** showed appreciable bioavailability due to poor cellular permeability.

Our GRK2 program started with high throughput screening (HTS) of the Janssen compound collection using a thermal shift (Thermofluor<sup>TM</sup>) assay. In this assay, compounds that bind to full-length human GRK2 protein were identified by observing a positive shift in  $T_m$  (the melting point). Positive controls were paroxetine (binding constant  $K_d = 2.98 \mu\text{M}$ , reported  $\text{IC}_{50} = 1.4$

$\mu\text{M}$ ) and **Takeda 103A** ( $K_d = 1.99 \text{ nM}$ ). There were 36 confirmed hits with  $K_d$  values ranging from 1.5 to 18.9  $\mu\text{M}$  after the first-round of HTS. One representative hit **1** (Figure 2) displayed micromolar affinity ( $K_d = 3.33 \text{ }\mu\text{M}$ ) in the Thermofluor<sup>TM</sup> binding assay and was further confirmed in the enzyme activity assay with an  $\text{IC}_{50}$  value of 4.1  $\mu\text{M}$ .

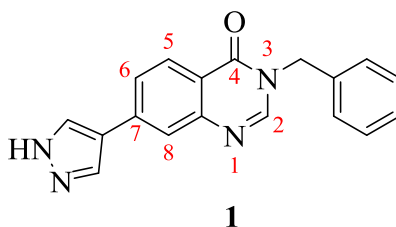


**Figure 2.** Structure of HTS hit

To gain an insight into the molecular basis for its binding, **1** was co-crystallized with human GRK2-G $\beta\gamma$  and the X-ray co-crystal structure was determined (PDB code: 7K7Z). As shown in Figure 3, the screening hit **1** occupied the ATP binding site and was a type-I kinase inhibitor. On the left-hand side, the pyrazole group at the C7 position forms two weak hydrogen bonds with the hinge of the kinase domain: one interacts the backbone carbonyl oxygen of Asp272 with a distance of 3.2Å and the other interacts the backbone NH of Met274 with a distance of 3.3Å. In the middle, the quinazolin-4(3H)-one scaffold forms an additional hydrogen bond with the backbone NH of Arg199 from the P-loop. On the right-hand side, the benzyl group sits in a hydrophobic pocket between the P-loop and the *alpha*-C helix.

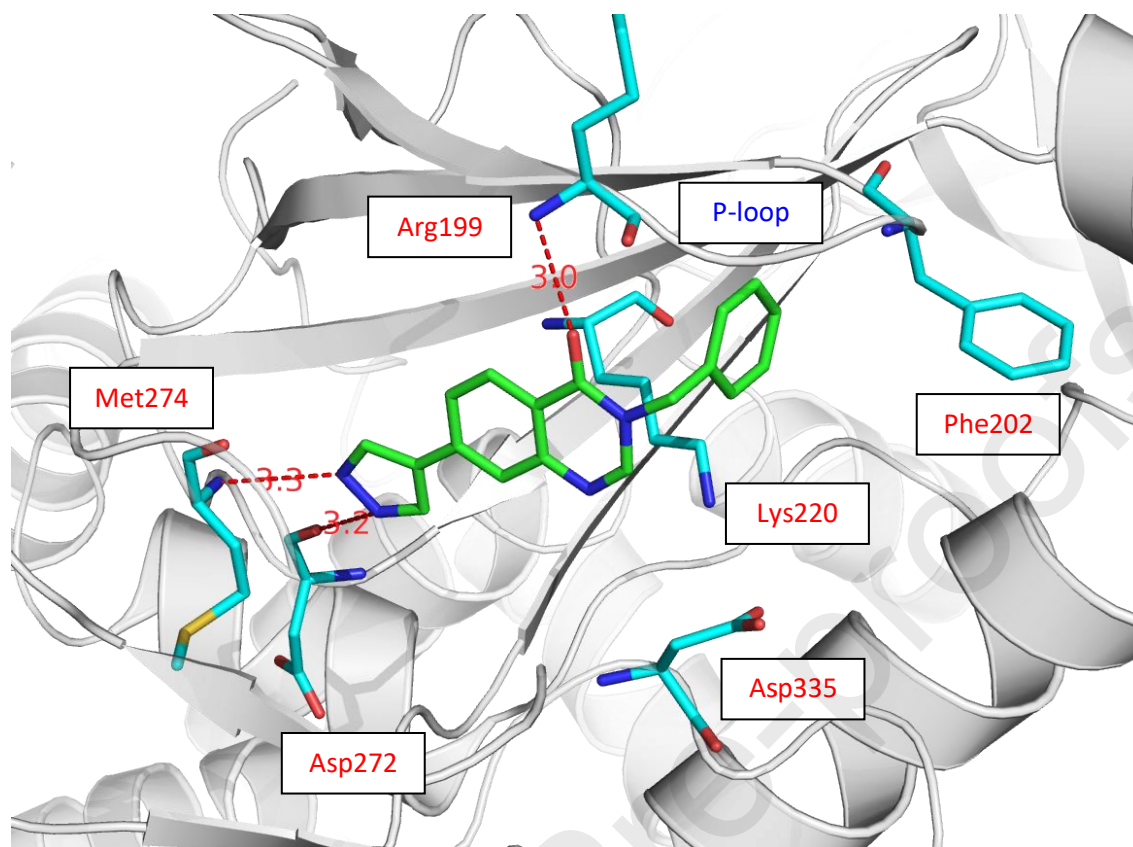


**Figure 3.** The X-ray complex structure of the hit **1** with GRK2-Gβγ (PDB code: 7K7Z). Key protein residues are represented by the stick model in cyan color. The ligand **1** is colored green. The hydrogen bonds are represented by red dashed lines with calculated distances.

It is noteworthy that the benzyl group is very close to the P-loop and could cause severe steric strain and result in weak binding affinity. This assumption has been validated by the electron density map where the densities of the benzyl and the P-loop are fused together (Figure 4).

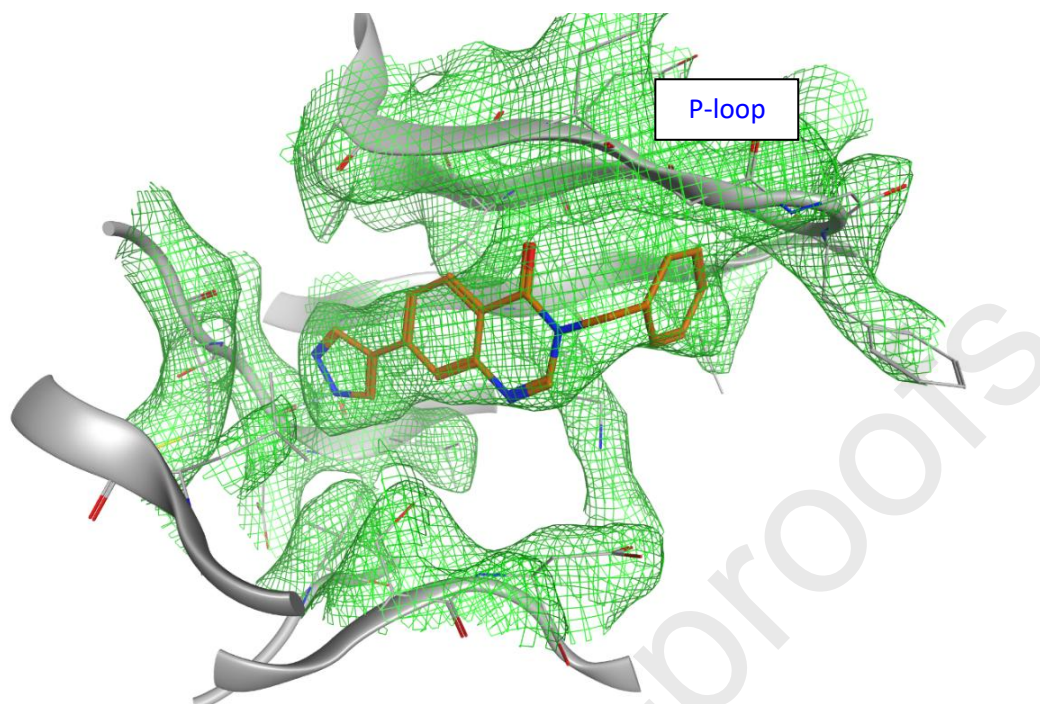


**Figure 4.** The electron density map shows that the densities of the benzyl group of the hit **1** and the P-loop of GRK2 are fused together (PDB code: 7K7Z). The electron density map is represented by the mesh grid in green. The hit **1** is colored orange and the GRK2 protein is represented by the ribbon in grey.

Our hit-to-lead optimization strategy was to design a molecule with stronger hydrogen bonds to the hinge region and without the steric strain with the P-loop. We envisioned that attaching various hinge binding motifs (e.g. heteroaromatic rings) at the **C6** position instead of the **C7** position would provide a molecule like **2** as shown in Figure 5, in which the binding conformation would be slightly shifted compared to **1** and lead to improved potency.

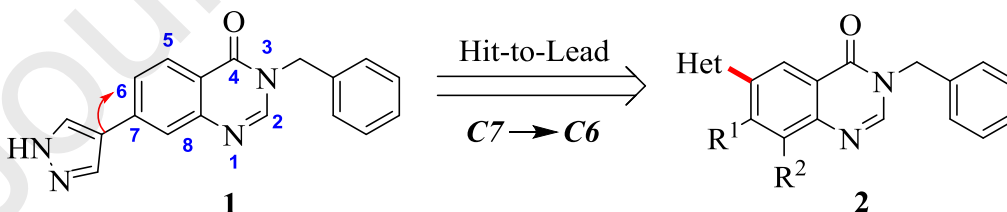
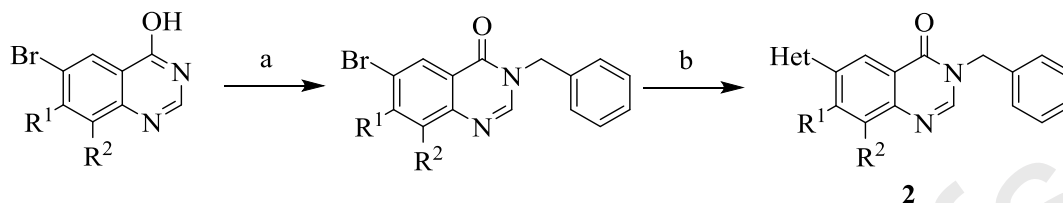


**Figure 5.** Hit-to-lead design strategy

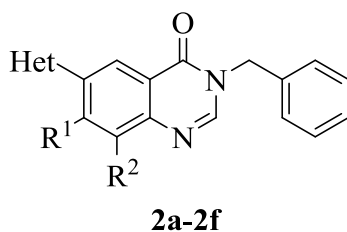
A short list of heteroaryl groups known to be hinge binders were incorporated at **C6** and the general synthesis of **2** is shown in Scheme 1. Benzylation of substituted bromoquinazolin-4-ol,

followed by Suzuki coupling of various heteroaryl boronic acid pinacol esters afforded the corresponding compound **2**.



**Scheme 1.** a) Benzylbromide,  $K_2CO_3$ , acetonitrile, 80%; b) Heteroaryl boronic acid pinacol ester,  $Pd(PPh_3)_4$ ,  $K_2CO_3$ , 1,4-dioxane, 50-60%.

The GRK2 inhibitory activity of newly synthesized compounds (**2a-2f**) was evaluated in a human GRK2 LANCE Ultra assay, which was used to test inhibitors against GRK2 in its inactive state (*see supporting material for details*) and is summarized in Table 1. Since there are seven G protein-coupled receptor (GPCR) kinases (GRKs)<sup>21</sup>: visual GRK subfamily (GRK1 and GRK7), the  $\beta$ -adrenergic receptor ( $\beta$ -AR) kinase subfamily (GRK2 and GRK3) and GRK4 subfamily (GRK4, GRK5 and GRK6), we also screened selected compounds **2a-2d** against GRK1 and GRK5 in the thermal shift assay ( $K_d$  data are shown in Table 1). The 5-pyrimidine analog (**2a**) and 3-pyrazole analog (**2c**) were inactive in the GRK2 assay up to 100  $\mu$ M. The 4-pyridine-analog **2b** showed only weak GRK2 inhibition ( $IC_{50} = 25 \mu$ M). However, the 4-pyrazole analog **2d** displayed potent GRK2 inhibitory activity ( $IC_{50} = 95$  nM), a 43-fold improvement compared to the screening hit **1**. More importantly, **2d** showed high selectivity against GRK1 ( $K_d = 14.5 \mu$ M) and GRK5 ( $K_d = 34.3 \mu$ M). Additional fluorine substitution at either C7 (**2e**) or C8 (**2f**) led to loss of activity against GRK2.

**Table 1.** GRK inhibitory activities of **2a-2f**

Cpd	Het	R <sup>1</sup>	R <sup>2</sup>	GRK2 IC <sub>50</sub> ( $\mu$ M) <sup>a</sup>	GRK1 K <sub>d</sub> ( $\mu$ M)	GRK5 K <sub>d</sub> ( $\mu$ M)
<b>1</b>	---	---	---	<b>4.1</b>	47.6	> 83.3
<b>2a</b>		H	H	>100	> 83.3	> 83.3
<b>2b</b>		H	H	25	> 83.3	> 83.3
<b>2c</b>		H	H	> 100	> 83.3	> 83.3
<b>2d</b>		H	H	<b>0.095</b>	14.5	34.3
<b>2e</b>		F	H	0.278	ND	ND
<b>2f</b>		H	F	0.472	ND	ND

<sup>a</sup>All IC<sub>50</sub> measurements are an average of three experiments run in duplicate. ND: Not determined.

The potency improvement for **2d** could be explained by a docking study using Glide<sup>22</sup> together with the X-ray structure information for **1** (PDB code: 7K7L). As illustrated in Figure 6, the quinazolin-4(3H)-one moiety of **2d** was flipped within the ATP binding site relative to **1**. Instead of interacting with the backbone NH of Arg199 in the case of **1**, the carbonyl group of **2d** formed a hydrogen bond with the side chain of Lys220. As a result, the benzyl group moved away from the P-loop and released the conformational strain. The model (orange color) was later validated by the X-ray co-crystal structure of **2d** in complex with human GRK2-G $\beta$  $\gamma$  (green color, Figure 6). In this co-crystal structure, **2d** formed two strong hydrogen bonds to the hinge with distances of 2.7Å and 3.0Å. The observed SAR for other compounds in Table 1 were

consistent with the predicted binding poses. For example, **2c** having a 3-pyrazole could only make one weak hydrogen bond to the hinge and **2a** having a 5-pyrimidine substituent cannot form any hydrogen bonds to the hinge. Both compounds did not show detectable inhibition up to 100  $\mu\text{M}$ . Interestingly, compound **2e** or **2f** with an additional fluorine atom at the  $\text{R}^1$  or the  $\text{R}^2$  position were 3- to 5-fold less potent than **2d**. A plausible explanation may be that the fluorine substituent is close to the backbone carbonyl of Ile197 resulting in electrostatic repulsion.

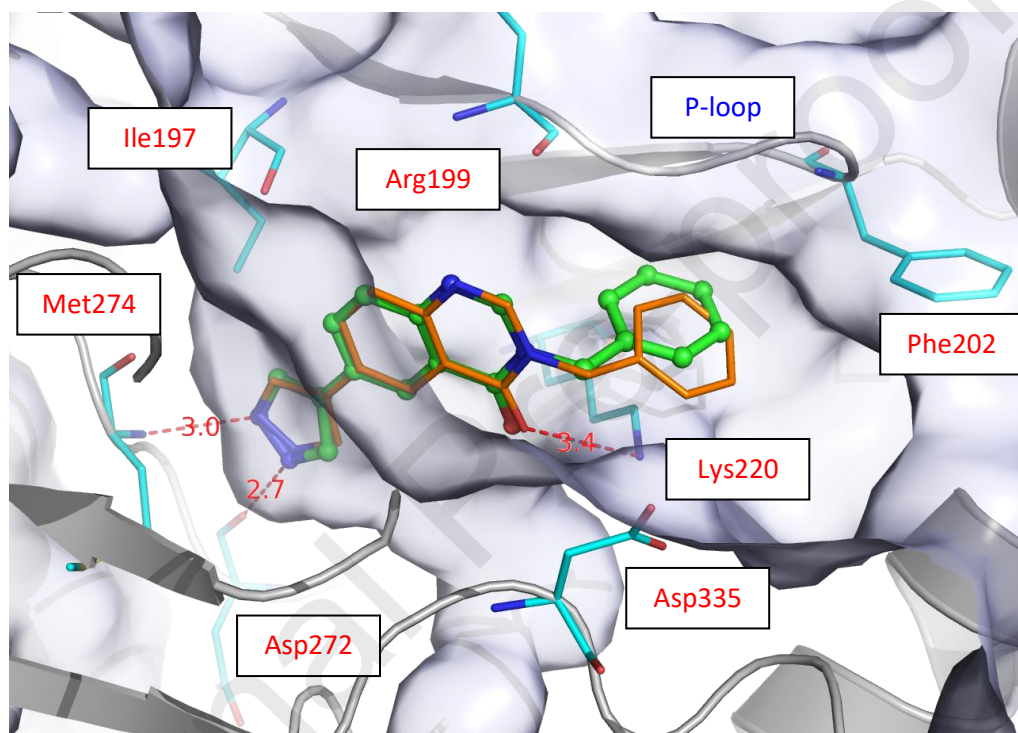


**Figure 6.** The binding poses of the lead **2d** in GRK2. The stick model in orange is the docking model, the ball-stick model in green is the X-ray co-crystal structure (PDB code: 7K7L).

With **2d** shown to form favorable interactions with the hinge, we then focused on optimizing the right-hand side of the molecule to further improve GRK2 potency. Takeda Pharmaceuticals has previously reported a series of potent but structurally distinct GRK2 inhibitors and the co-crystal structure of a prototypical inhibitor Takeda **115h**<sup>17</sup> with human GRK2-G $\beta\gamma$  (orange color, PDB code: 3PVU, Figure 7). The structural overlay of our own lead compound **2d** with Takeda **115h** shows that both phenyl groups on the right-hand side (underneath the P-loop) are perfectly aligned (Figure 7). The extra amide carbonyl of **115h** forms a strong hydrogen bond with the

backbone NH of Phe202 and its additional phenyl group interacts with the hydrophobic pocket. All these additional interactions make Takeda **115h** a very potent GRK2 inhibitor ( $IC_{50}=18$  nM).

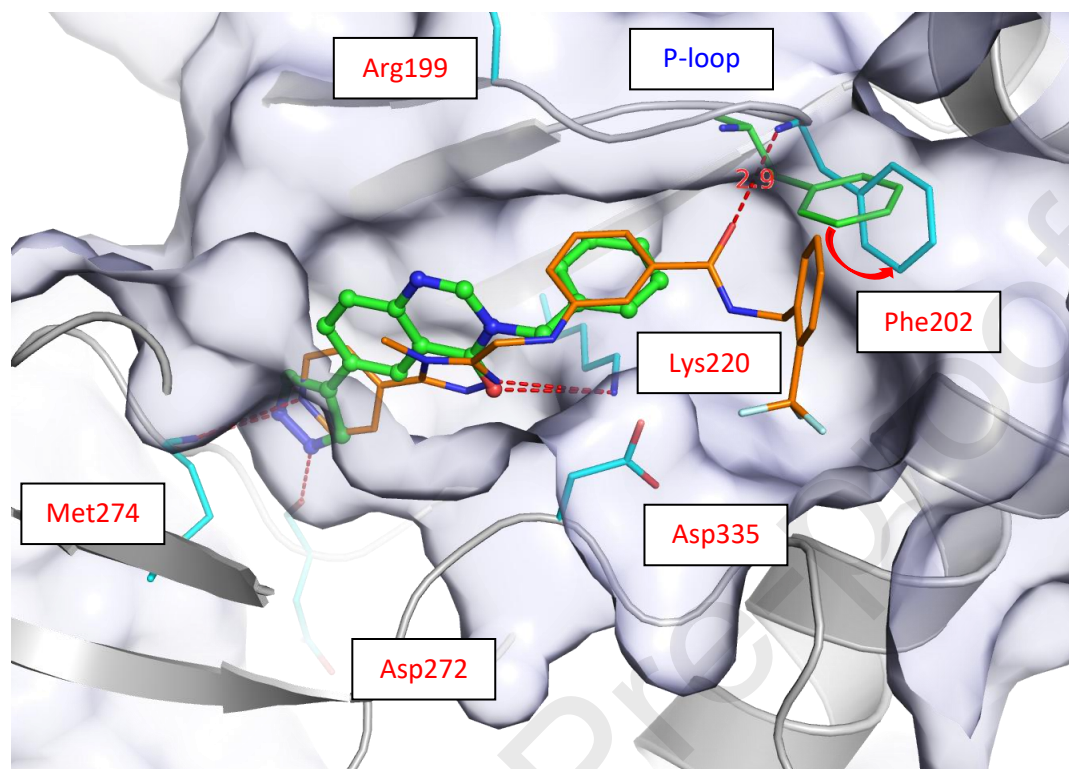
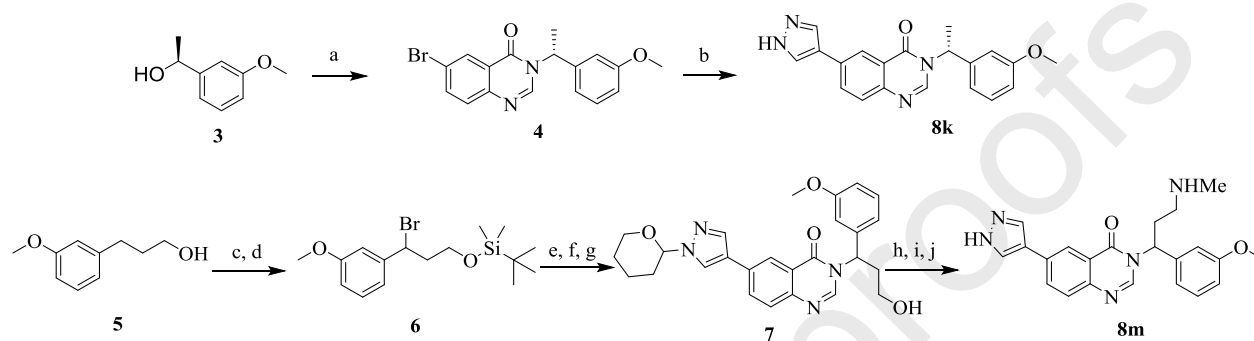


**Figure 7.** The overlay of the X-ray structure of **2d** (PDB code: 7K7L, green) with Takeda **115h**<sup>17</sup> (PDB code: 3PVU, orange).

We therefore hypothesized that the structure-activity relationships (SAR) from the Takeda series could be applied to the **2d** scaffold. A small library of compounds (**8a-8m**) was designed, synthesized, and the GRK2 inhibitory activity determined, as summarized in Table 2. Compounds **8a-8j** were synthesized following the previous procedures shown in Scheme 1, where the appropriate benzylbromide and 6-bromoquinazolin-4(3H)-one or 7-bromophthalazin-1(2H)-one was used. The preparation of **8k** is illustrated in Scheme 2. Mitsunobu reaction of (*S*)-1-(3-methoxyphenyl)ethan-1-ol with 6-bromoquinazolin-4(3H)-one provided intermediate **4** in 37.4% isolated yield. Suzuki coupling of **4** with 4-(4,4,5,5-tetramethyl-1,3,2-dioxaborolan-2-yl)-1H-pyrazole afforded **8k**. Following the same protocol, **8l** was obtained starting from (*R*)-1-(3-methoxyphenyl)ethan-1-ol. The synthesis of **8m** is also illustrated in Scheme 2. TBS protection of 3-(3-methoxyphenyl)propan-1-ol (**5**), followed by *N*-bromosuccinimide (NBS) bromination

provided intermediate **6**. Alkylation of **6** with 6-bromoquinazolin-4(3H)-one, followed by Suzuki coupling with 1-(tetrahydro-2H-pyran-2-yl)-4-(4,4,5,5-tetramethyl-1,3,2-dioxaborolan-2-yl)-1H-pyrazole, and TBAF-mediated removal of the TBS group generated the alcohol **7**. Conversion of **7** into its mesylate, followed by reaction with methylamine, and TFA-mediated deprotection afforded **8m** as a racemic mixture.

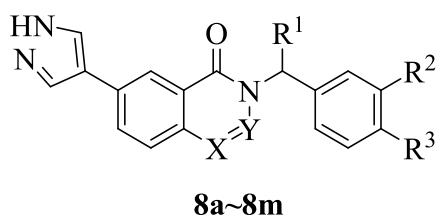


**Scheme 2.** a) 6-Bromoquinazolin-4(3H)-one, PPh<sub>3</sub>, DIAD, THF, 37.4%; b) 4-(4,4,5,5-Tetramethyl-1,3,2-dioxaborolan-2-yl)-1H-pyrazole, Pd(PPh<sub>3</sub>)<sub>4</sub>, K<sub>2</sub>CO<sub>3</sub>, 1,4-dioxane, 31.4%; c) TBDMSCl, imidazole, DMF, 72.3%; d) NBS, BPO, CCl<sub>4</sub>, 80°C, 39.0%; e) 6-Bromoquinazolin-4(3H)-one, K<sub>2</sub>CO<sub>3</sub>, acetone, 81.5%; f) 1-(Tetrahydro-2H-pyran-2-yl)-4-(4,4,5,5-tetramethyl-1,3,2-dioxaborolan-2-yl)-1H-pyrazole, Pd(PPh<sub>3</sub>)<sub>4</sub>, K<sub>2</sub>CO<sub>3</sub>, DMF, water, 75.4%; g) tetrabutylammonium fluoride (TBAF), THF, 98.3%; h) MsCl, Et<sub>3</sub>N, DCM, 91.2%; i) MeNH<sub>2</sub>, MeOH, 80 °C, 67.9%; j) TFA, DCM, 23.7%.

Three analogs (**8a**, **8b**, and **8c**) with various amide moieties (R<sup>2</sup> group) at the *meta*-position of the phenyl ring were potent GRK2 inhibitors (IC<sub>50</sub> < 10 nM). The amide carbonyl was expected to make a hydrogen bond with Phe202 in the P-loop, as observed in the Takeda series. Surprisingly, **8d** with a *para*-2,6-difluorobenzylformamide substitution was >2,000-fold less potent than the corresponding *meta*-substituted **8c**. The potency loss could be attributed to a steric clash between the *para*-2,6-difluorobenzylformamide group and the protein surface near the P-loop. Regardless of potency, compounds **8a**–**8d** all exhibited poor permeability as judged by their low A→B P<sub>app</sub> values (0.44~0.85) in the MDCK permeability assay. Interestingly, the 4-fluorophenoxy-substituted analog **8e** showed modest GRK2 potency (IC<sub>50</sub> = 78 nM) but improved permeability (A→B P<sub>app</sub>: 7.73). A couple of smaller groups (**8f** and **8g**) with an ether linker were explored to further increase permeability and **8f** indeed showed high permeability but modest GRK2 potency (IC<sub>50</sub> = 206 nM). In contrast, **8g** with a methoxy group at the *meta*-

position was a potent GRK2 inhibitor with an  $IC_{50}$  value of 6 nM, which was comparable to compounds **8a~8c** with much larger  $R^2$  substituents.

Journal Pre-proofs

**Table 2.** GRK2 inhibitory activities and permeability data for **8a-8m**<sup>a</sup>

Cpd	X/Y	R <sup>1</sup>	R <sup>2</sup>	R <sup>3</sup>	GRK2 IC <sub>50</sub> (μM)	A→B P <sub>app</sub> (cm/s*10 <sup>-6</sup> ) <sup>b</sup>
<b>8a</b>	N/CH	H		H	0.009	0.44
<b>8b</b>	N/CH	H		H	< 0.010	0.57
<b>8c</b>	N/CH	H		H	< 0.010	0.85
<b>8d</b>	N/CH	H	H		20.0	0.66
<b>8e</b>	N/CH	H		H	0.078	7.73
<b>8f</b>	N/CH	H		H	0.206	24.2
<b>8g</b>	N/CH	H		H	0.006 <sup>c</sup>	20.6
<b>8h</b>	CH/N	H		H	0.019	53.2
<b>8i</b>	N/CH	H		F	0.018	10.1
<b>8j</b>	N/CH	H	F		2.75	12.3
<b>8k</b>	N/CH	( <i>R</i> )-Me		H	0.013	37.8
<b>8l</b>	N/CH	( <i>S</i> )-Me		H	2.11	ND
<b>8m</b> ( <i>rac</i> )	N/CH			H	0.012	< 0.34

<sup>a</sup>All IC<sub>50</sub> measurements are averages of three separate experiments run in duplicate. <sup>b</sup>MDR1-MDCK permeability assay; <sup>c</sup>GRK2 LANCE assay. ND: Not determined.

Molecular modelling studies suggested that the ether oxygen is close to the backbone NH of Phe202 and could make favorable electrostatic interactions and a water-mediated hydrogen bond (Figure 8). The phthalazin-1(2H)-one analog **8h** with a *meta*-methoxy group also exhibited good GRK2 inhibitory activity ( $IC_{50} = 19$  nM) and excellent permeability. However, introducing a fluorine substituent next to the methoxy (**8i**) led to a 3-fold loss in potency. Analogous to compound **8d** with a bulky substituent at the *para*-position, the smaller *para*-methoxy-substituted analog **8j** lost considerable GRK2 inhibitory activity ( $IC_{50} = 2.75$   $\mu$ M). Adding a methyl group at the benzylic position ( $R^1$ ), as in compound **8k**, did not enhance potency. Furthermore, compound **8l** with an *S*-methyl group lost GRK2 inhibitory activity. It is believed that the *S*-methyl interferes with the hydrogen bonding interaction between the 2,3-quinazolin-4(3H)-one and Lys220.

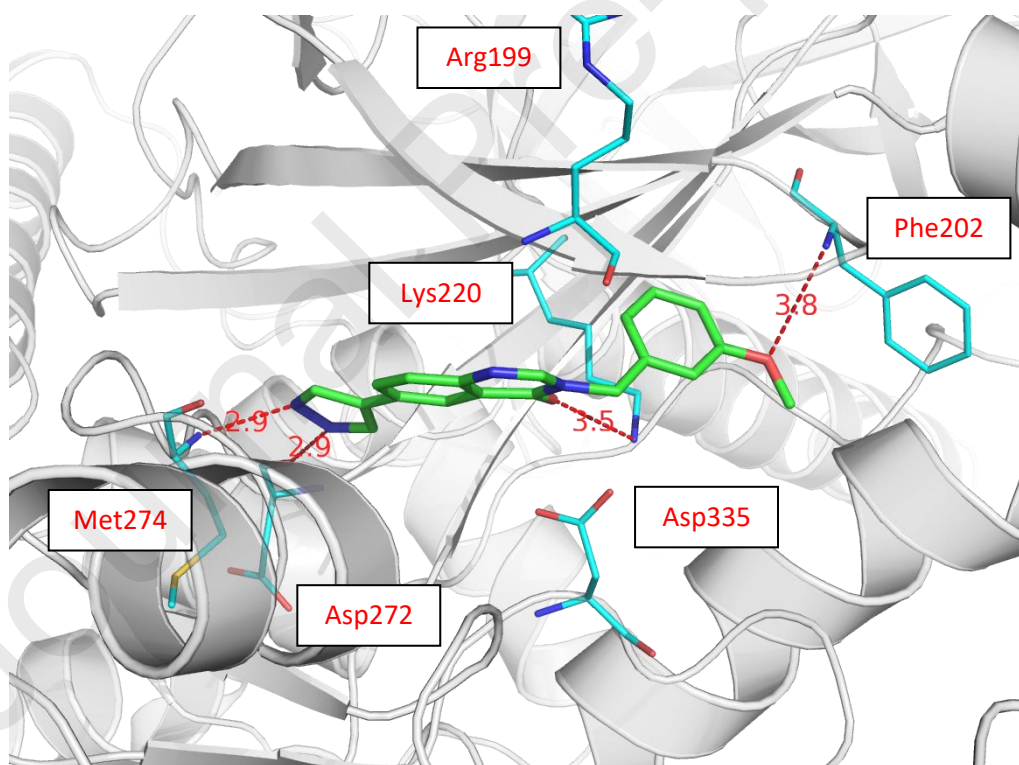


**Figure 8.** The predicted model of **8g** in which the ether is close to the backbone NH of Phe202

Compound **8m** was designed for two purposes. First, the side chain secondary amine moiety ( $R^1$ ) of **8m** was expected to increase aqueous solubility. Second and more importantly, the terminal amine would be expected to form a salt-bridge with the acid group of Asp335 and make a hydrogen bond with the backbone carbonyl of Asn322 based on molecular modelling (Figure 9, *R*-configuration is shown). The compound **8m** (tested as a racemic mixture) displayed good GRK2 inhibition ( $IC_{50} = 12$  nM) but did not show significant improvement due to the entropy loss from the flexible chain and the de-solvation penalty from the binding of the charged amine group. The drawback for **8m** is that it has poor permeability in the MDCK assay.

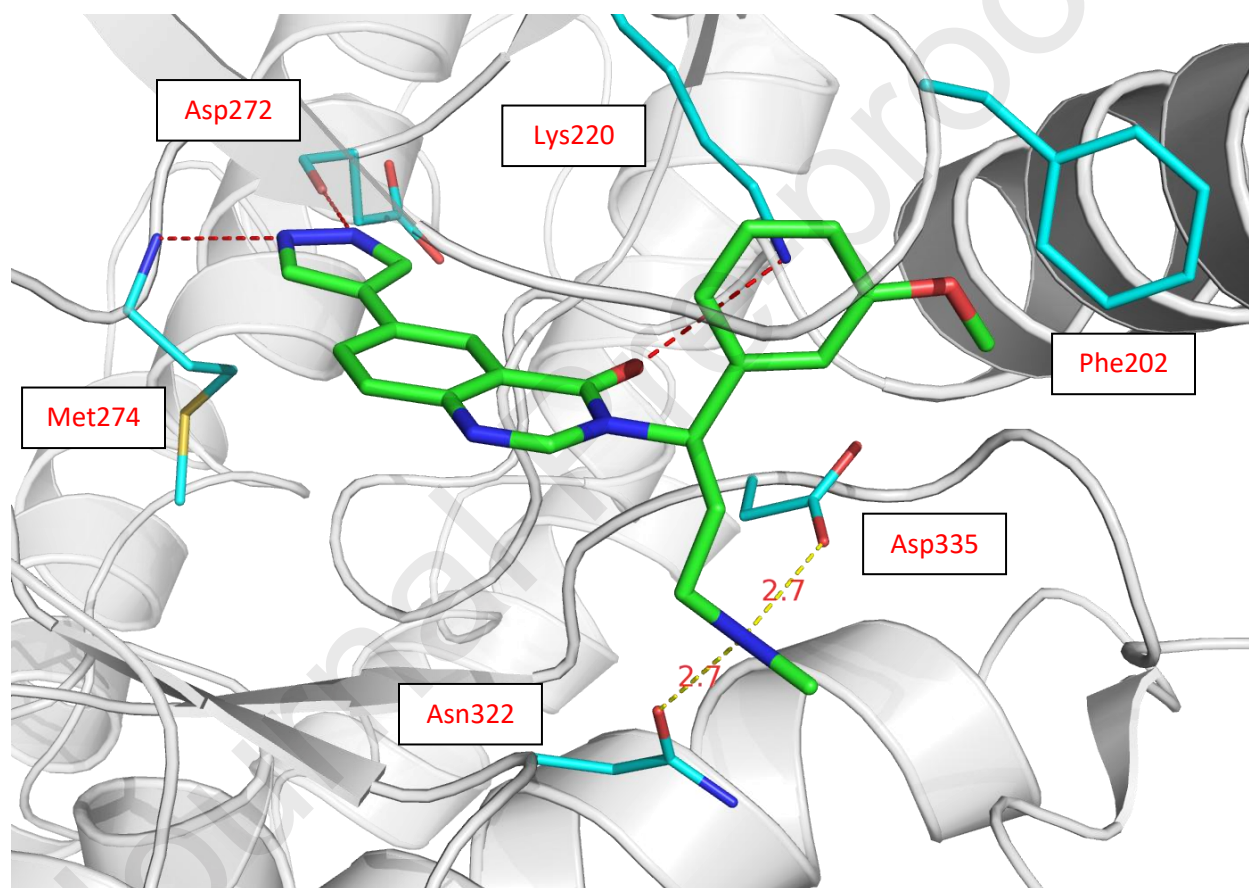


**Figure 9.** The predicted model of **8m** interacting with GRK2. The N-methylethanamine side chain forms a salt-bridge with Asp335 and a hydrogen bond with Asn322

With good GRK2 potency and cell permeability, compounds **8g** and **8h** were selected for screening against a limited kinase panel including several closely related AGC-family kinases and Aurora-A. The  $IC_{50}$  data for both **8g** and **8h** obtained by Eurofins Pharma Discovery Services are summarized in Table 3. The GRK2  $IC_{50}$  values for **8g** (10 nM) and **8h** (19 nM) were

consistent with our internal data shown in Table 2. Both compounds were quite selective for GRK2 versus GRK1, GRK5, GRK6, GRK7, PKA, PKB $\alpha$ , PKC $\alpha$ , PKC $\beta$ 1, and CaMKII $\beta$ . However, **8g** was equally potent in inhibiting Aurora-A (IC<sub>50</sub> = 11 nM). Interestingly, **8h** showed improved selectivity for GRK2 versus Aurora-A (7.2-fold), ROCK-1 (67-fold), and Rsk1 (166-fold). We therefore selected **8h** for further *in vitro* cellular evaluation.

**Table 3.** Kinase selectivity of **8g** and **8h**

Kinase	IC <sub>50</sub> (nM) for <b>8g</b>	IC <sub>50</sub> (nM) for <b>8h</b>
GRK2	10	19
GRK1	>10000	>10000
GRK5	4497	>10000
GRK6	3270	>10000
GRK7	9137	>10000
PKA	855	4880
PKB $\alpha$	1449	>10000
PKC $\alpha$	>10000	>10000
PKC $\beta$ 1	9068	>10000
CaMKII $\beta$	3846	>10000
ROCK-1	246	1271
Aurora-A	11	137
Rsk1	483	3151

It has been known that stimulation of  $\beta$ -ARs activate the canonical adenylate cyclase pathway via the Gs alpha subunit leading to cAMP accumulation.<sup>23</sup> To demonstrate that GRK2 canonical kinase activity is directly involved in regulation of  $\beta$ -AR mediated Gs activation, we conducted an isoproterenol-mediated cAMP accumulation assay in HEK293-hGRK2 cells. Pre-incubation with **8h** enhanced  $\beta$ -AR-mediated cAMP accumulation in HEK293 cells stably overexpressing GRK2 (Figure 10). This result suggests that inhibition of GRK2 kinase activity can potentiate  $\beta$ -AR signaling.

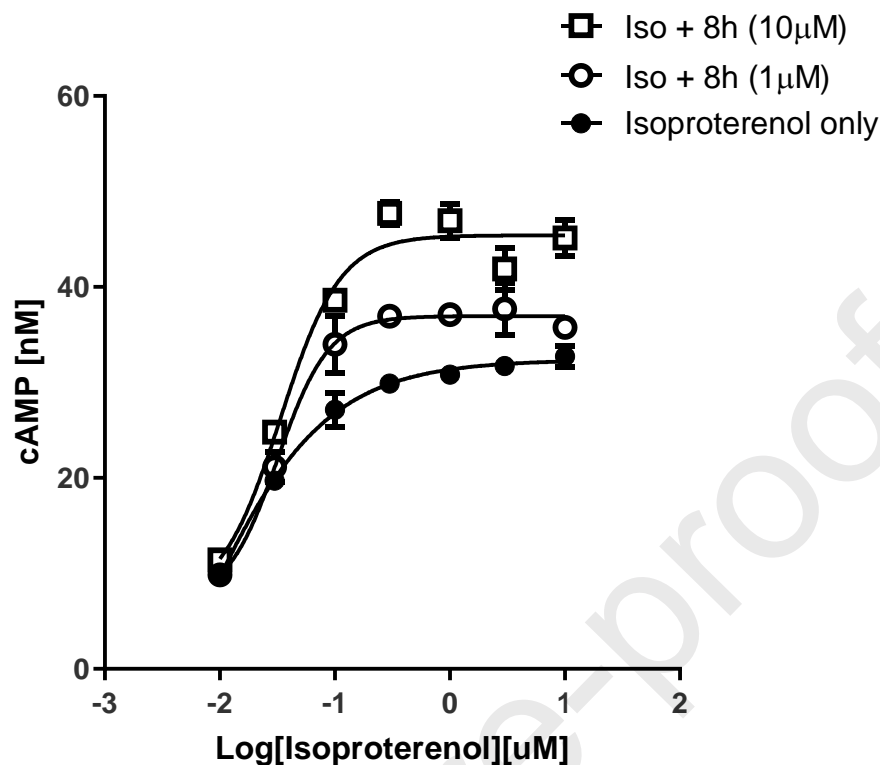


**Figure 10.** Compound **8h** enhanced isoproterenol-mediated cAMP production in HEK293-hGRK2 cells

Compound **8h** was further evaluated in a synchronously beating human stem cell-derived cardiomyocyte (HSC-MC) assay (Table 4). At concentrations of 0.1, 1 and 10  $\mu\text{M}$  in the presence of isoproterenol, **8h** increased the beating rate of the  $\text{Ca}^{2+}$  transients measured in HSC-CMs, compared to cells treated with isoproterenol alone. The increase in beating rate is reflecting cAMP accumulation, a surrogate pharmacodynamic (PD) marker of GRK2 inhibition.

**Table 4.** Effects of **8h** at 0.1, 1 or 10  $\mu\text{M}$  in the presence of 1  $\mu\text{M}$  isoproterenol on calcium transient morphology of synchronously beating cardiomyocytes, expressed as a change from baseline, measured with the FDSS ( $n = 8$ ) at time point of 27 mins. Values are medians of actual units and change from baseline in percent.

Parameter	Treatment	Change from baseline as %
-----------	-----------	---------------------------

<b>Beat rate (min<sup>-1</sup>)</b>	isoproterenol (1 $\mu$ M)	12
	<b>8h</b> (0.1 $\mu$ M) + iso (1 $\mu$ M)	18*
	<b>8h</b> (1.0 $\mu$ M) + iso (1 $\mu$ M)	24*
	<b>8h</b> (10 $\mu$ M) + iso (1 $\mu$ M)	24*

\*Statistically significant values ( $p < 0.01$ ). **8h** at 0.1, 1, or 10  $\mu$ M plus isoproterenol (1  $\mu$ M) vs. isoproterenol (1  $\mu$ M) alone, respectively.

Compound **8h** was evaluated in a pharmacokinetic study in C57BL mice (Table 5). Administration of a single 2 mg/kg dose intravenously or a single 10 mg/kg dose orally revealed that **8h** had moderate clearance ( $CL = 29.1$  ml/min/kg) and distributed extensively outside the plasma, with a volume of distribution  $\sim 2.77$  times greater than total body water. Compound **8h** was notable for rapid absorption, a high oral  $C_{max}$  of 4.96  $\mu$ M, and oral bioavailability of 65.3%. With potent GRK2 inhibitory activity, *in vitro* cellular activity, and good oral PK profile, **8h** will serve as an interesting tool compound for future *in vivo* studies in animal models of HF.

**Table 5.** Pharmacokinetic parameters of **8h** in C57BL Mice<sup>a</sup>

Cpd	Dose i.v./p.o. <sup>b</sup> (mg/kg)	$CL_p$ (ml/min/kg)	$Vd_{ss}$ (L/kg)	i.v. $t_{1/2}$ (h)	p.o. $t_{1/2}$ (h)	$C_{max}$ ( $\mu$ M)	$t_{max}$ (h)	Oral AUC ( $\mu$ M.h.kg)	F (%)
<b>8h</b>	2/10	29.1	2.01	1.01	2.41	4.96	0.83	11.89	65.3

<sup>a</sup> $CL_p$ , plasma clearance;  $Vd_{ss}$ , volume of distribution at steady state;  $t_{1/2}$ , terminal half-life;  $C_{max}$ , maximum concentration;  $t_{max}$ , time of maximum concentration; AUC, area under plasma concentration vs time curve; F, bioavailability. <sup>b</sup>Formulation for both intravenous (i.v.) and oral (p.o.): 20% HP $\beta$ CD.

In summary, we have successfully applied structure-based design, synthesis, and systematic exploration of SAR to optimize a weak screening hit **1** and identify a potent and selective GRK2 inhibitor **8h**, which possesses pharmacokinetics suitable for oral administration. Compound **8h** has been demonstrated to potentiate isoproterenol mediated cAMP accumulation in HEK293-hGRK2 cells. More importantly, **8h** enhances the beating rate of the Ca<sup>2+</sup> transients in synchronously beating human stem cell-derived cardiomyocytes.

## Acknowledgements

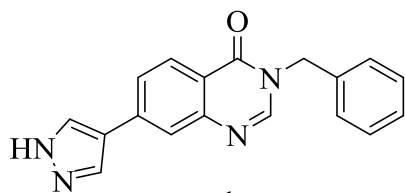
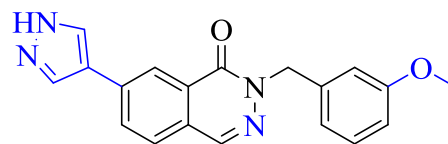
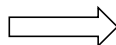
We would like to thank Dr. Mark Macielag for reviewing this manuscript. We also thank Pharmaron Inc. for conducting the pharmacokinetic study.

## References and Notes

- (1) Kemp, CD; Conte, JV. The pathophysiology of heart failure. *Cardiovasc. Pathol.* **2012**, 21, 365–371.
- (2) Chemaly, ER; Hajjar, RJ; Lipskaia, L. Molecular targets of current and prospective heart failure therapies. *Heart* **2013**, 99, 992– 1003.
- (3) Heart Failure Fact Sheet. [https://www.cdc.gov/heartdisease/heart\\_failure.htm](https://www.cdc.gov/heartdisease/heart_failure.htm) (accessed April 6th, 2020).
- (4) Pfeffer, MA; Swedberg, K; Granger, CB; Held, P; McMurray, JJ; Michelson, EL; Olofsson, B; Ostergren, J; Yusuf, S. Effects of candesartan on mortality and morbidity in patients with chronic heart failure: the CHARM-Overall programme. *Lancet* **2003**, 362, 759–766.
- (5) Satwani, S; Dec, GW; Narula, J.  $\beta$ -Adrenergic Blockers in Heart Failure: Review of Mechanisms of Action and Clinical Outcomes. *J. Cardiovasc. Pharmacol. Ther.* **2004**, 9, 243–255.
- (6) Chaggar, PS; Malkin, CJ; Shaw, SM; Williams, SG, Channer, KS. Neuroendocrine effects on the heart and targets for therapeutic manipulation in heart failure. *Cardiovasc Ther.* **2009**, 27(3):187-93.
- (7) Port, JD; Bristow, MR. Altered beta-adrenergic receptor gene regulation and signaling in chronic heart failure. *J Mol Cell Cardiol.* **2001**, 33(5):887-905.
- (8) Eschenhagen, T. Beta-adrenergic signaling in heart failure adapt or die. *Nat. Med.* **2008**, 14, 485–487.
- (9) Lymperopoulos, A; Rengo, G; Funakoshi, H; Eckhart, AD; Koch, WJ. Adrenal GRK2 upregulation mediates sympathetic overdrive in heart failure. *Nat. Med.* **2007**, 13, 315–323.
- (10) Iaccarino, G; Barbato, E; Cipolletta, E; De Amicis, V; Margulies, KB; Leosco, D; Trimarco, B; Koch, WJ. Elevated myocardial and lymphocyte GRK2 expression and activity in human heart failure. *Eur. Heart J.* **2005**, 26, 1752–1758.

- (11) Harding, VB; Jones, LR; Lefkowitz, RJ; Koch, WJ; Rockman, HA. Cardiac  $\beta$ ARK1 inhibition prolongs survival and augments  $\beta$  blocker therapy in a mouse model of severe heart failure. *Proc. Natl. Acad. Sci. U. S. A.* **2001**, 98, 5809–5814.
- (12) Raake, PW; Vinge, LE; Gao, E; Boucher, M; Rengo, G; Chen, X; DeGeorge, BR, Jr; Matkovich, S; Houser, SR; Most, P; Eckhart, AD; Dorn, GW, II; Koch, WJ. G protein-coupled receptor kinase 2 ablation in cardiac myocytes before or after myocardial infarction prevents heart failure. *Circ. Res.* **2008**, 103, 413–422.
- (13) Raake, PW; Schlegel, P; Ksienzyk, J; Reinkober, J; Barthelmes, J; Schinkel, S; Pleger, S; Mier, W; Haberkorn, U; Koch, WJ; Katus, HA; Most, P; Müller, OJ. AAV6. $\beta$ ARKct cardiac gene therapy ameliorates cardiac function and normalizes the catecholaminergic axis in a clinically relevant large animal heart failure model. *Eur Heart J.* **2013**, 34(19):1437-47.
- (14) Murga, C; Arcones, AC; Cruces-Sande, M; Briones, AM; Salaices, M; Mayor, FJ. G Protein-Coupled Receptor Kinase 2 (GRK2) as a Potential Therapeutic Target in Cardiovascular and Metabolic Diseases. *Front. Pharmacol.* **2019**, 10:112.
- (15) Guccione, M; Ettari, R; Taliani, S; Settimo, FD; Zappalà, M; Grasso, S. G-Protein-Coupled Receptor Kinase 2 (GRK2) Inhibitors: Current Trends and Future Perspectives. *J. Med. Chem.* **2016**, 59, 9277–9294
- (16) Tesmer, JJG; Tesmer, VM; Lodowski, DT; Steinhagen, H; Huber, J. Structure of Human G Protein-Coupled Receptor Kinase 2 in Complex with the Kinase Inhibitor Balanol. *J. Med. Chem.* **2010**, 53, 1867–1870.
- (17) Okawa, T; Aramaki, Y; Yamamoto, M; Kobayashi, T; Fukumoto, S; Toyoda, Y; Henta, T; Hata, A; Ikeda, S; Kaneko, M; Hoffman, ID; Sang, B; Zou, H; Kawamoto, T. Design, Synthesis, and Evaluation of the Highly Selective and Potent G-Protein-Coupled Receptor Kinase 2 (GRK2) Inhibitor for the Potential Treatment of Heart Failure. *J. Med. Chem.* **2017**, 60, 6942–6990
- (18) Thal, DM; Homan, KT; Chen, J; Wu, EK; Hinkle, PM; Huang, ZM; Chuprun, JK; Song, J; Gao, E; Cheung, JY; Sklar, LA; Koch, WJ; Tesmer, JJG. Paroxetine Is a Direct Inhibitor of G Protein-Coupled Receptor Kinase 2 and Increases Myocardial Contractility. *ACS Chem. Biol.* **2012**, 7, 1830–1839.

- (19) Waldschmidt, HV; Homan, KT; Cruz-Rodríguez, O; Cato, MC; Waninger-Saroni, J; Larimore, KM; Cannavo, A; Song, J; Cheung, JY; Kirchhoff, PD; Koch, WJ; Tesmer, JJG; Larsen, SD. Structure-Based Design, Synthesis, and Biological Evaluation of Highly Selective and Potent G Protein-Coupled Receptor Kinase 2 Inhibitors. *J. Med. Chem.* **2016**, 59, 3793–3807
- (20) Waldschmidt, HV; Homan, KT; Cato, MC; Cruz-Rodríguez, O; Cannavo, A; Wilson, MW; Song, J; Cheung, JY; Koch, WJ; Tesmer, JJG; Larsen, SD. Structure-Based Design of Highly Selective and Potent G Protein-Coupled Receptor Kinase 2 Inhibitors Based on Paroxetine. *J. Med. Chem.* **2017**, 60, 3052–3069
- (21) Lefkowitz, RJ. G Protein-coupled receptor kinases. *Cell*, **1993**, 74, 409-412.
- (22) Friesner, RA; Murphy, RB; Repasky, MP; Frye, LL; Greenwood, JR; Halgren, TA; Sanschagrin, PC; Mainz, DT. Extra precision glide: docking and scoring incorporating a model of hydrophobic enclosure for protein-ligand complexes, *J. Med. Chem.*, **2006**, 49, 6177-6196.
- (23) Bristow MR, Hershberger RE, Port JD, Minobe, W; Rasmussen, R. Beta 1- and beta 2-adrenergic receptor-mediated adenylate cyclase stimulation in nonfailing and failing human ventricular myocardium. *Mol Pharmacol.* **1989**, 35(3):295-303.

**1****HTS hit**GRK2 IC<sub>50</sub> = 4.1 μM**8h**GRK2 IC<sub>50</sub> = 19 nM

Oral PK profile in C57BL mice (10 mg/kg)

C<sub>max</sub> = 4.96 μMAUC<sub>inf</sub> = 11.89 μM\*h\*kg

F = 65.3%